applied sciences

MDPI

Review

Cr(VI) Sorption from Aqueous Solution: A Review

Angelo Fenti [1], Simeone Chianese [1,2,*], Pasquale Iovino [2,3], Dino Musmarra [1,2] and Stefano Salvestrini [2,3,*]

1 Department of Engineering, University of Campania "Luigi Vanvitelli", Via Roma 29, 81031 Aversa (CE), Italy; angelo.fenti@unicampania.it (A.F.); dino.musmarra@unicampania.it (D.M.)
2 Environmental Technologies, University Spin Off of University of Campania "Luigi Vanvitelli", Department of Environmental, Biological and Pharmaceutical Sciences and Technologies via Vivaldi, 43, 81100 Caserta, Italy; pasquale.iovino@unicampania.it
3 Department of Environmental, Biological and Pharmaceutical Sciences and Technologies, University of Campania "Luigi Vanvitelli", via Vivaldi 43, 81100 Caserta, Italy
* Correspondence: simeone.chianese@unicampania.it (S.C.); stefano.salvestrini@unicampania.it (S.S.)

Received: 26 August 2020; Accepted: 15 September 2020; Published: 17 September 2020

Abstract: Hexavalent chromium (Cr(VI)) in water systems is a major hazard for living organisms, including humans. The most popular technology currently used to remove Cr(VI) from polluted water is sorption for its effectiveness, ease of use, low cost and environmental friendliness. The electrostatic interactions between chromium species and the sorbent matrix are the main determinants of Cr(VI) sorption. The pH plays a central role in the process by affecting chromium speciation and the net charge on sorbent surface. In most cases, Cr(VI) sorption is an endothermic process whose kinetics is satisfactorily described by the pseudo second-order model. A critical survey of the recent literature, however, reveals that the thermodynamic and kinetic parameters reported for Cr(VI) sorption are often incorrect and/or erroneously interpreted.

Keywords: hexavalent chromium; sorption; sorption isotherm; sorption kinetics; pseudo first order model; pseudo second order model; sorption thermodynamics

1. Introduction

Environmental pollution is currently a cause of serious concern worldwide. Anthropogenic activities produce increasing amounts of processing waste and effluents that contain a diversity of pollutants, including harmful heavy metals [1]. Among these, chromium is well known for its mutagenic and carcinogenic effects [2]. Chromium naturally occurs in the earth's crust and water bodies but its level in the environment tends to increase in association with anthropogenic activities such as metallurgy, wood processing, and production of inorganic chemicals, printed circuit boards and dyes [3,4].

Chromium predominantly occurs in the +3 (Cr(III)) and +6 (Cr(VI)) oxidation states. Cr(VI) is highly soluble in aqueous systems and exhibits higher soil mobility and higher toxicity than Cr(III) [5]. In fact, the hexavalent form of chromium is highly toxic and carcinogenic, while the trivalent form is innocuous and may even be used as a micronutrient in certain organisms [6]. Cr(VI) has a high diffusion and dissolution capacity in the tissues [7]. Its compounds can be absorbed by humans through the skin and respiratory system and rapidly diffuse in the body due to their ability to enter the erythrocytes and bind to hemoglobin. Documented harmful effects of Cr(VI) in humans include lung cancer, respiratory problems, renal failure, weakening of the immune system, skin lesions, genetic damage and infertility [8]. Cr(VI) species enter the cells across non-specific anionic channels, thanks to structural analogy with sulphate and phosphate ions. Cr^{5+} complexes, produced by reduction of Cr(VI) within the cells, may react with endogenous H_2O_2 to generate potentially mutagenic OH radicals [9].

Recognizing the multi-faceted harmful effects of Cr(VI) on living organisms, the US Environmental Protection Agency (US-EPA) has established a maximum level in drinking and surface water of 0.015 and 0.1 mg L^{-1}, respectively [10].

The removal of Cr(VI) from water is an issue that is drawing increasing attention within the scientific community. Among a diversity of methods tested so far, sorption is the most popular because it is fast, relatively inexpensive and easy to use. Not surprisingly, therefore, a considerable effort has been done for the development of novel sorbents for Cr(VI) removal since the last century [11–16]. Here we present a critical review of the experimental work performed on Cr(VI) sorption in the last decade, with emphasis on proposed mechanisms and thermodynamic and kinetic aspects.

2. Cr(VI) Behavior in Solution and Proposed Sorption Mechanisms: Effect of pH

Sorption is a general term encompassing a diversity of processes such as adsorption, absorption, ion exchange and surface precipitation, as well as a diversity of mechanisms depending on the physicochemical properties of sorbate and sorbent. Being a surface phenomenon, sorption usually increases with an increase of the surface area of the sorbent [17–19]. Other factors, notably the pH and the surface charge of the sorbent, may play a leading role in the process [8,20].

Cr(VI) is present in water in different oxyanionic forms (e.g., $HCrO_4^-$, CrO_4^{2-} and $Cr_2O_7^{2-}$) or as undissociated chromic acid, H_2CrO_4, the relative abundance of each species being strongly related to the pH. The equilibria that contribute most significantly to Cr(VI) speciation in water are reported below [21–23]:

$$H_2CrO_4 \rightleftarrows H^+ + HCrO_4^- \qquad K_1 = 0.37 \tag{1}$$

$$HCrO_4^- \rightleftarrows H^+ + CrO_4^{2-} \qquad K_2 = 3.2 \times 10^{-7} \tag{2}$$

$$2HCrO_4^- \rightleftarrows Cr_2O_7^{2-} + H_2O \qquad K_3 = 35.5 \tag{3}$$

where K_1, K_2 and K_3 are the equilibrium constants of the three reactions. The first two equilibria are pH-dependent whereas the third only depends on total Cr(VI) concentration. The effect of pH and total Cr(VI) concentration (based on Equations (1)–(3)) on Cr(VI) species distribution, is shown in Figure 1 in a range of concentrations commonly found in contaminated water systems [24].

As can be seen from Figure 1, $HCrO_4^-$ and CrO_4^{2-} are the most abundant species at acid and basic pH, respectively. Due to the negative net charge of Cr(VI) oxyanions, Cr(VI) sorption is expected to involve electrostatic interactions or anion exchange with positively-charged sorbent sites [6,24,25]. The uptake of Cr(VI) should be favored by a pH below the point of zero charge, which would impart the sorbent a net positive charge [20]. Chromium sorption should be less efficient under alkaline conditions than in acidic medium, not only because of electrostatic repulsion between chromium oxyanions and negatively-charged sites on sorbent surface but also because of competition with OH^- for sorbent sites.

In line with the analysis above, most papers on Cr(VI) report a decreasing sorption capacity with increasing pH. A typical trend of sorption capacity vs. pH is shown in Figure 2 [20,25,26].

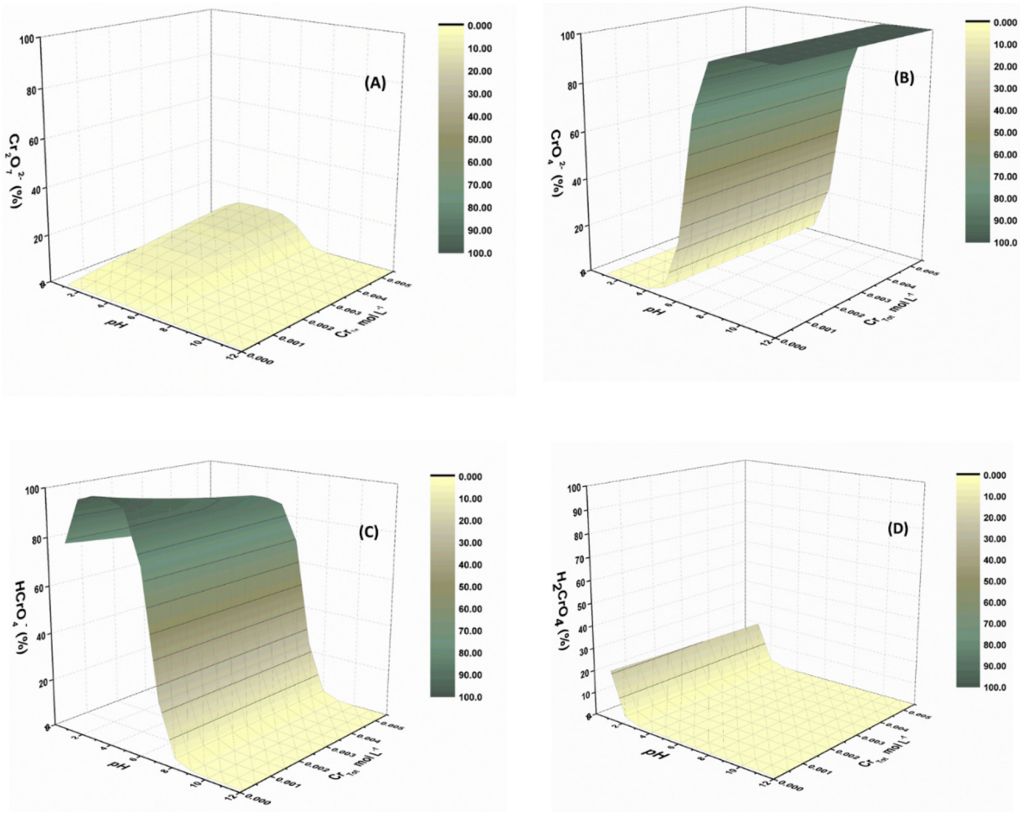

Figure 1. Cr(VI) species distribution (%) as a function of pH and total Cr(VI) concentration: (**A**) $Cr_2O_7^{2-}$; (**B**) CrO_4^{2-}; (**C**) H_2CrO_4; (**D**) $HCrO_4^-$.

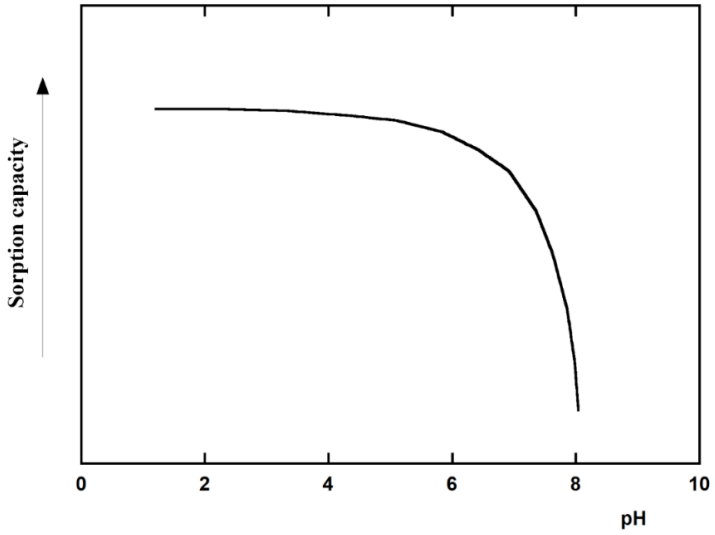

Figure 2. Typical decreasing trend of Cr(VI) sorption capacity vs. pH.

Shi et al. [20], for example, investigated the sorption performance of the anion-exchange resins D301, D314 and D354 for Cr(VI). The authors ascribed the observed sorption behavior with varying pH (similar to that shown in Figure 2), to an anion exchange process between Cr species and OH^- anions associated to -$N(CH_3)_2$ functional groups of the resins, according to the following reactions:

$$R - OH + HCrO_4^- \rightleftharpoons R - HCrO_4 + OH^- \quad (4)$$

$$2R - OH + CrO_4^{2-} \rightleftharpoons R_2 - CrO_4 + 2OH^- \quad (5)$$

$$2R - OH + 2HCrO_4^- \rightleftharpoons R_2 - Cr_2O_7 + 2OH^- + H_2O \quad (6)$$

$$2R - OH + Cr_2O_7^{2-} \rightleftharpoons R_2 - Cr_2O_7 + 2OH^- \quad (7)$$

where R is the resins' matrix.

The authors reported that the amount of Cr(VI) sorbed in acidic condition was double than in alkali condition. An obvious explanation is that in acidic condition the exchanged OH- reacts with H^+, thus promoting the forward reactions in Equations (4)–(7). At alkaline pH values, the sorption of Cr(VI) is hampered by competition between CrO_4^{2-} and OH^- for binding sites. At high pH (i.e., in excess of OH^-), this competitive effect leads to a drastic reduction of Cr(VI) uptake (Figure 2).

Kyzas et al. [25] investigated the sorption of Cr(VI) on chitosan derivatives cross-linked and grafted with amino and carboxyl groups. The authors observed a sorption trend with increasing pH similar to that observed by Shi et al. [20]. The researchers ascribed the higher uptake of Cr(VI) in acidic conditions to the protonation of amino groups in the chitosan sorbents, which would induce an electrostatic attraction to oxyanion Cr(VI) species. The same study [25] also reported a slightly lower Cr(VI) removal efficiency at pH 2 relatively to pH 4, which was attributed to chitosan instability at this pH.

An alternative mechanism for water purification from Cr(VI) involves reduction to Cr(III), a process in which pH also plays a central role [6,27,28]. Janos et al. [6] studied the reduction and immobilization of Cr(VI) with oxyhumolite and iron humate. The authors found that the amount of Cr(VI) removed from the solution in the presence of oxyhumolite decreased with increasing pH (Figure 3A).

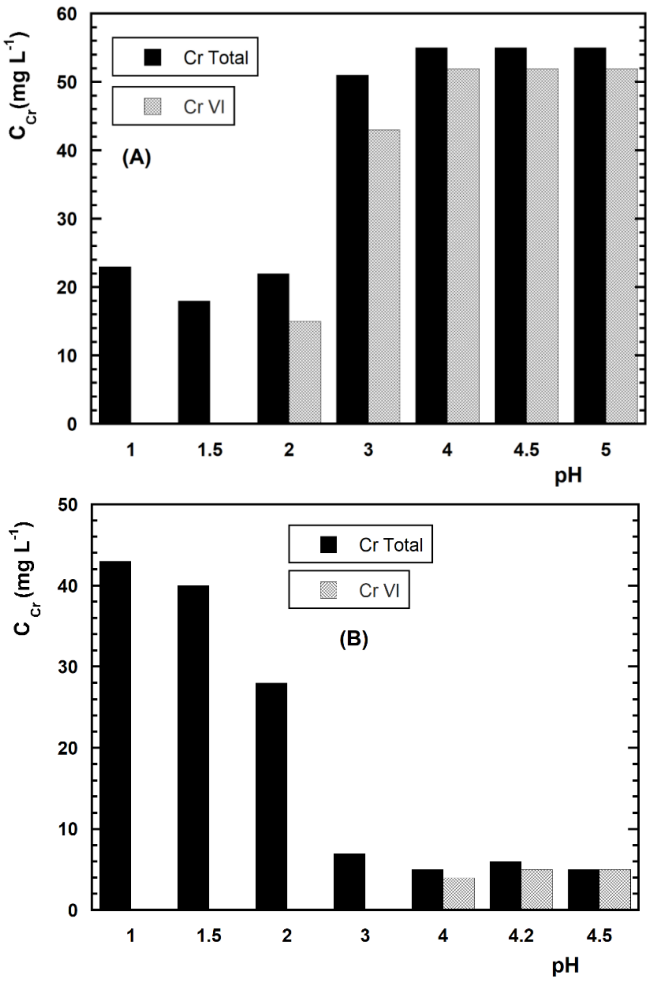

Figure 3. Residual chromium concentration in solution as a function of pH. Sorbent used: (**A**) oxyhumolite; (**B**) iron humate. Adapted from Janos et al. [6].

Two mechanisms were proposed to account for that, involving direct and indirect reduction of Cr(VI). In the former mechanism, Cr(VI) is directly reduced to Cr(III) in the aqueous phase by contact with electron-donor groups of the sorbent; Cr(III) thus formed may be sorbed by cation-exchange or remain in solution. The indirect reduction pathway proposed postulates that Cr(VI) in the oxyanionic form initially binds via electrostatic interaction to the positively charged sorbent surface, then undergoes reduction by adsorbent electron-donor groups and is finally released in solution or remains bound to the sorbent. The study by Janos et al. [6] clearly identified two processes: Cr(VI) reduction to Cr(III) favored at lower pH, and Cr(III) retention by the sorbent favored at higher pH. Interestingly, a somewhat different trend was observed when using iron humate as sorbent (Figure 3B). The authors related this trend to the presence of iron compounds in the sorbent material that might be able to reduce Cr(VI) over a wide pH range. The resulting Cr^{3+} cations might be retained on the sorbent by several mechanisms, such as ion-exchange, covalent binding or surface precipitation and co-precipitation of Fe^{3+}/Cr^{3+} hydroxides. It is worth mention that the pH used by Janos et al. [6] is below 5, hence their results are not strictly comparable with those shown in Figures 2 and 4.

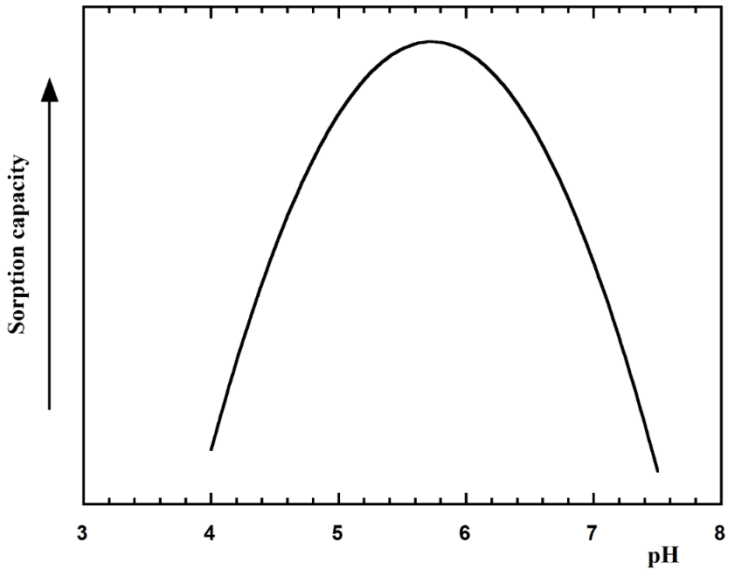

Figure 4. Typical bell-shaped trend of sorption capacity as a function of pH.

Campos [28] examined the performance of powder carbon steel for Cr(VI) removal from water. This author found a higher Cr removal efficiency with decreasing pH, probably due to Cr(VI) reduction to Cr(III) coupled with oxidation of Fe to Fe^{3+}. Fe^{3+} and Cr^{3+} thus produced could react forming mixed oxide with low solubility and consuming H^+. On the other hand, chromate and Fe^{2+} ions may react and form mixed Cr and Fe oxides generating H^+ release. The following Equations (8) and (9) illustrate some of the reactions discussed above:

$$Fe + CrO_4^{2-} + 0.5H_2O + 2H^+ \rightarrow Fe(OH)_3 + 0.5Cr_2O_3 \quad (8)$$

$$6Fe^{2+} + 2CrO_4^{2-} + 13H_2O \rightarrow 6Fe(OH)_3 + Cr_2O_3 + 8H^+ \quad (9)$$

A similar reduction in the sorption capacity with the increasing pH was observed by Kantar et al. [22], who investigated the sorption and reduction of Cr(VI) to Cr(III) using pyrite (FeS_2). The mechanism proposed by the authors was quite complex, involving a number of simultaneous or sequential steps, including pyrite dissolution, precipitation of oxidation products, protonation/deprotonation of chromium and of oxidized surfaces. A decrease in Cr(VI) removal efficiency associated with increasing pH was ascribed, at least in part, to pyrite surface passivation due to the accumulation of oxidation products. Under acidic conditions, pyrite releases Fe^{2+} which may

reduce Cr(VI) to Cr(III) in the solution phase. Interestingly, the authors also suggested that Fe^{2+} ions could also be sorbed onto pyrite, thus activating a cyclic redox mechanism that would further favors Cr(VI) reduction. The overall reaction pathway proposed is:

$$3FeS_2 + 14HCrO_4^- + 50H^+ \rightarrow 3Fe^{2+} + 6SO_4^{2-} + 14Cr^{3+} + 32H_2O \quad (10)$$

Di Natale et al. [29] used an additive-competitive Langmuir model to describe the effects of both pH and temperature on the chromium adsorption capacity of a commercial granular activated carbon, accounting for the chromium ion speciation. They highlighted that the optimal pH conditions were derived from the compensation between higher Cr(VI) ionization, favored at higher pH, and lower competition with OH- ions, favored at lower pH.

Ozer et al. [26] investigated the sorption of Cr(VI) by free and immobilized biomass (*Pediastrum boryanum*) and observed the typical decreasing sorption trend with increasing pH (Figure 2). This result was related by the authors to deprotonation of amino groups at the sorbent surface, which would hamper the electrostatic binding of chromium oxyanions.

A distinctive effect of pH on the sorption of Cr(VI) was observed by Koujalagi and co-workers [30] using Tulsion A-27(MP) resin (Figure 4). The sorption capacity vs. pH followed a bell-shaped curve with a maximum in the pH range 5–6 (Figure 4). The authors ascribed the fall of sorption capacity at high pH to sorbent surface passivation of the adsorbent surface by precipitation of hydroxides. In contrast, the decrease at low pH was ascribed to competition of H^+ with Cr(VI) for sorption sites.

In the study carried out by Chakrava et al. [31], husk of *Lathyrus sativus* was used as a sorbent for Cr(VI). It was found that the presence of functional groups such as $^-NH_2$, ^-OH and PO_4^{3-} on the biomass surface markedly affected Cr(VI) uptake. More in detail, the authors suggested that the binding of Cr(VI) involved hydrogen bonds with amino and hydroxyl groups, or electrostatic interactions with protonated phosphate groups.

A pH effect similar to that displayed in Figure 4 was also found by Wu and co-workers [32] using chitosan-xylan-TiO_2 adsorbent. The authors attributed the low sorption of Cr(VI) in acidic solution (pH 4) to electrostatic repulsion between the protonated functional groups of the sorbent and positively charged chromium ions. This explanation is not convincing because, as discussed above, at pH 4 Cr(VI) is prevalently present as oxyanion. An alternative explanation might be the structural alteration of the sorbent surface in acidic environment and consequent loss of sorption capacity [33–35]. A third mechanism possibly contributing to reduce Cr(VI) sorption at low pH (<2) might be the formation of oligomers of chromium species such as $Cr_3O_{10}^{2-}$ and $Cr_4O_{13}^{2-}$ [36,37].

Gheju and coworkers studied the sorption of Cr(VI) onto MnO_2 [24]. A pH rise from 5.9 to 8.1 remarkably reduced Cr(VI) removal. The pH dependence of the process was ascribed to: (i) an increase in the negative net charge of the sorbent with increasing pH (being the point of zero charge pH_{PZC} = 5.8) and consequent increase of electrostatic repulsion between the sorbent surface and chromium oxyanions; (ii) higher competition between chromium oxyanions and OH^- for positive sorption sites with increasing pH.

A bell shape curve such as that shown in Figure 4 was also reported by Hans et al. [38] for the sorption of Cr(VI) onto MIEX®, a magnetic ion exchange resin. A maximum sorption capacity was observed in the pH range 4–6. The authors ascribed the reduction in sorption capacity at lower and higher pH to competition between Cr(VI) and H^+ and between Cr(VI) and OH^-, respectively.

Cr(VI) sorption capacity by siderite ($FeCO_3$) in anoxic aqueous solution was lower at pH 4 than at pH 5 and 6 [39]. This phenomenon was ascribed by the authors to reduction of Cr(VI) to Cr(III) by Fe^{2+} on the mineral surface or in solution.

Cr(VI) sorption capacity of schwertmannite attained a maximum at pH 6.0 [40]. Cr(VI) sorption by schwertmannite was mainly attributed to ion exchange between Cr(VI) and structural SO_4^{2-}, a process possible because the Cr(VI) species and SO_4^{2-} have the same charge and similar sizes.

A novel biochar-supported zero-valent iron stabilized by carbomethyl cellulose was recently developed and used for Cr(VI) sorption experiments [41]. These experiments revealed that the

uptake/removal of Cr(VI) occurred via a complex mechanism involving electrostatic attraction, reduction and surface complexation. The main reactions of the proposed mechanism are reported below:

$$3Fe^0 + Cr_2O_7^{2-} + 14H^+ \rightarrow 3Fe^{2+} + 2Cr^{3+} + 7H_2O \quad (11)$$

$$HCrO_4^- + 7H^+ + 3e^- \leftrightarrow Cr^{3+} + 4H_2O \quad (12)$$

$$3Fe^{2+} + HCrO_4^- + 7H^+ \rightarrow 3Fe^{3+} + Cr^{3+} + 4H_2O \quad (13)$$

$$Fe^{2+} + Cr_2O_4^{2-} \leftrightarrow FeCr_2O_4(s) \quad (14)$$

$$2Cr^{3+} + 6OH^- \leftrightarrow 2Cr(OH)_3(s) \leftrightarrow Cr_2O_3(s) + 3H_2O \quad (15)$$

$$xCr^{3+} + (1-x)Fe^{3+} + 3H_2O \rightarrow (Cr_xFe_{1-x})(OH)_3(s) + 3H^+ \quad (16)$$

$$xCr^{3+} + (1-x)Fe^{3+} + 3OH^- \rightarrow (Cr_xFe_{1-x})(OH)_3(s) \quad (17)$$

3. Equilibrium and Thermodynamic Aspects of Cr(VI) Sorption

3.1. Sorption Isotherms

The sorption equilibrium of Cr(VI), as for any other sorbate, is generally investigated using the sorption isotherms [42]. These are obtained by plotting the sorbed amount of Cr(VI) per unit mass of sorbent (q_e) at equilibrium against the initial Cr(VI) concentration (C_e).

The isotherm models most frequently applied for describing Cr(VI) sorption are the Langmuir model and the Freundlich model [43].

The Langmuir model [44] (Equation (18)) is a simplistic model applicable under the assumptions that (i) the sorbate encompasses a finite number of energetically equivalent sites arranged in a superficial monolayer, and (ii) the solution behaves ideally (i.e., the solution is diluted enough for solute activity being approximated by concentration), and there are no intermolecular interactions among the free solute and/or sorbate molecules [45,46]:

$$q_e = \frac{q_m K_L C_e}{1 + K_L C_e} \quad (18)$$

where q_m and K_L are the maximum sorption capacity and the Langmuir equilibrium constant, respectively.

The Freundlich model [47] (Equation (19)) is a power function empirical model especially useful for the practical purpose of describing sorption equilibrium data not including a sorption saturation level as the Langmuir model demands:

$$q_e = K_F {C_e}^N \quad (19)$$

where K_F and N are empirical constants. It has been suggested that the value of the N parameter gives information on the heterogeneity of sorbent sites: values of N significantly lower than 1 (concave downward isotherms) would reflect high heterogeneity, whereas values of $N \cong 1$ (linear isotherms) would be indicative of a homogeneous energetic distribution of sorption sites. It is important to note that N is a dimensionless parameter. This notwithstanding, N is sometimes erroneously reported with units of L mg^{-1} [48,49].

With few exceptions [18,50–52], if compared to, the Langmuir model fits better than the Freundlich model the experimental data for Cr(VI) sorption. Liu et al. [53] obtained a higher correlation coefficient using the Langmuir model for modelling the sorption isotherms of Cr(VI) sorption by poly(N^1,N^1,N^3,N^3-tetraallylpropane-1,3-diaminium chloride) (PTAPDAC). A better performance of the Langmuir model was confirmed by Anandaraj et al. [54] using native and chemically modified green macroalgae *Codium tomentosum* biomass as a sorbent. Similar results were obtained by Mikhaylov et al. [8] using Al/Fe oxyhydroxide composite powders, Sutkowy and Klosowsky [55] using the

green alga *Pseudopediastrum boryanum* and many other authors using minerals [40,56], synthetized materials [1,7,10,20,57,58] or biosorbents [26,27,48,59].

In some cases [6,25,60], a semi-empirical hybrid Langmuir-Freundlich model, also known as Sips model [61], has been used for modelling isotherm equilibrium data:

$$q_e = \frac{q_m K_{LF} {C_e}^N}{1 + K_{LF} {C_e}^N} \quad (20)$$

where K_{LF} is a constant.

The Sips model generally gives better fitting results than either the Langmuir or the Freundlich model. This is not surprising, because the Sips model is a more general (and therefore adaptable) equation that, for $N = 1$ or for high Cr(VI) initial concentration, reduces to the Langmuir model whereas for sufficient low Cr(VI) concentration (i.e., $1 >> K_{LF}\ {C_e}^N$) reduces to the Freundlich model (with $K_F = q_m K_{LF}$).

In rare cases, the equilibrium sorption data exhibited unusual trends not amenable to modelling by any of the isotherm equations described above. For example, Gheju and coworkers [24] reported a bell-shaped isotherm curve for the sorption of Cr(VI) onto MnO_2. Normally, sorption capacity increases with increasing sorbate initial concentration and eventually reaches a plateau that corresponds to the saturation level of the sorbent. In contrast, the sorption capacity of the sorbent was higher at low chromium concentration and declined at higher concentration. The authors attributed this unusual behavior to $HCrO_4^-$ dimerization to $Cr_2O_7^{2-}$. Because of its larger volume, $Cr_2O_7^{2-}$ has more difficult access to sorption sites, thus reducing the sorption capacity of MnO_2.

3.2. Maximum Sorption Capacity

A most important parameter for evaluating sorbent efficiency is the maximum (saturation) sorption capacity, q_m, as determined from the plateau level of the experimental isotherm. A list of values of q_m for different sorbents is given in Table 1. It is important to note that the q_m values reported here may not be strictly comparable because, as discussed above, the Cr(VI) sorption capacity may vary with operative conditions such as pH and temperature. The highest maximum sorption capacity for Cr(VI), 12.0 mmol g^{-1}, was reported by Setshedi et al. [62] for a polypyrrole graphene oxide nanocomposite. High values of q_m were also found for nanosilica immobilized-fungi (q_m = 10.1 mmol g^{-1}) [36], grafted aerobic granular sludge (q_m = 7.7 mmol g^{-1}) [60], and chitosan/poly(vinyl amine) cryogel (q_m = 6.1 mmol g^{-1}) [63].

Table 1. Thermodynamic data for Cr(VI) sorption.

Sorbent Type	q_m (mmol g^{-1})	K_L (L $mmol^{-1}$)	$q_m K_L$ (L g^{-1})	K_F ($mmol^{1-N}$ L^N g^{-1})	N	T (°C)	$\Delta H°$ (kJ mol^{-1})	$\Delta S°$ (J K^{-1} mol^{-1})°	$\Delta G°$ (kJ mol^{-1})	pH	Ref.
Magnetic ion exchange resin	1.781	181	322.4	/	/	25	/	/	/	4	[38]
Zero-valent iron-carboxymethyl cellulose	2.163	16.59	35.88	1.856	0.230	25	/	/	/	5.6	[41]
Siderite	/	/	/	1.408	0.130	20	/	/	/	5	[39]
Zirconium oxide-alginate beads	0.200	1.633	0.327	0.109	0.466	25	21.224	163	−27.430	5	[58]
Mg–Al hydrotalcite	1.383	22.26	30.79	1.723	0.40	Room	/	/	/	6	[35]
Anion exchanger chitosan/poly(vinyl amine)	6.114	0.974	5.955	2.673	0.345	25	61.11	219	−4.18	5.5	[63]
Cross linked-chitosan-polyaniline	3.446	5.928	20.43	2.943	0.227	30	13.46	10	−9.18	4.2	[64]
Mg-Zn-Al hydrotalcite derived oxides	0.961 *	/	/	/	/	30	/	/	/	6	[65]
Fe (II)-modified natural zeolite	5.769×10^{-3} *	/	/	/	/	Room	/	/	/	5.5	[66]
Anion-exchange resins	3.005	81.19	244.0	3.084	0.151	27	0.016	39.88	−4.498	5	[20]
MnO_2	0.016 *	/	/	/	/	20	−22.52	−50.40	−8.08	6.9	[24]
Schwert- mannite	1.890	3.04	5.746	0.97	0.313	25	/	/	/	6	[40]
Iron/carbon Fe/C composites	0.981	5.782	5.672	0.998	0.483	Room	/	/	/	5	[27]
Cereal by-product carbon	2.300 *	/	/	/	/	20	0.7142	−94.8	28.479	6	[4]
Calcinated Al/Fe oxide–oxyhydroxide	0.074	123.4	9.132	0.0837	0.104	Room	/	/	/	6.7	[67]
Polyethylenimine grafted sludge	7.721	4.16	32.12	2.241	0.48	25	/	/	/	5.5	[60]
Nannochloris oculata	0.725	0.530	0.384	0.215	0.67	/	/	/	/	2	[50]
Amine-functionalized corn stalk	4.370	10.92	47.72	3.474	0.128	45	96.79	30	−7.16	3	[68]
Dolomite	0.192	14.14	2.715	0.203	0.304	20	−13.21	−22.47	−6.617	2	[51]
Acinetobacter junii VITSUKMW2	0.436	115.5	50.36	0.0506	0.389	27	−3.764	0.018	−1.989	2	[48]
Polypyrrole graphene oxide	12.030	104	1251	11.68	0.029	25	78.417	282.67	−7.287	2	[62]
Al/Fe oxide–oxyhydroxide	0.070	54.6	3.82	0.103	0.26	/	/	/	/	5.4	[8]
Sargassum bevanom	0.763	1158.8	884.2	0.484	0.342	20	28.656	115	−5.256	3	[19]
Iron oxide-activated carbon	0.155	8.84	1.370	0.119	0.37	25	49.906	168.3	−0.293.3	2	[49]
Ash gourd (*Benincasa hispida*) waste	0.360 *	/	/	0.472	0.25	28	/	/	/	1	[69]
Chitosan–xylan–TiO_2	1.867	1.217	2.272	0.904	0.50	45	4.44	35.98	−7.00	7	[32]
Teff straw	1.656	86.30	142.9	2.166	0.277	45	34.25	150.07	−13.468	2	[70]
Sawdust	0.870	47.32	41.17	12.24	0.813	40	34.67	124.1	−4.2140	3	[52]
Codium tomentosum	0.105	11.44	1.201	0.228	0.622	20	/	/	/	2	[54]
Vinylpyridine divinylbenzene	4.130	2.777	11.47	/	/	25	/	/	/	2	[71]
β-Cyclodextrin-polyurethane	0.045	52	2.34	9.739	0.25	25	/	/	/	3	[72]
Husk of *Lathyrus sativus*	0.940	4.493	4.223	0.214	0.073	30	/	/	/	2	[31]

Table 1. *Cont.*

Sorbent Type	q_m (mmol g^{-1})	K_L (L mmol^{-1})	$q_m K_L$ (L g^{-1})	K_F (mmol^{1-N} L^N g^{-1})	N	T (°C)	$\Delta H°$ (kJ mol^{-1})	$\Delta S°$ (J K^{-1} mol^{-1})°	$\Delta G°$ (kJ mol^{-1})	pH	Ref.
Organoclay	0.045	38.06	1.713	0.698	0.885	25	/	/	/	2	[56]
Resin Tulsion A-27	1.620	0.370	0.599	2.64	0.144	50	−9.9	10.2	−13.2	5.5	[30]
Nanosilica-immobilized fungi	10.120	0.0267	0.270	0.804	0.442	25	/	/	/	2	[36]
Solid biodiesel waste residue	2.530	0.936	2.368	1.119	0.431	30	−9.34	−23.27	−2.040	2	[73]
Fe-modified peanut husk	0.637	0.52	0.331	0.199	0.557	30	−9087	−32.488	753.94	2	[74]
Pediastrum boryanum	0.585	11.08	6.482	0.456	0.254	25	44.5	251	−17.4	2	[26]
Trewia nudiflora	5.656	11.08	62.67	4.917	0.273	30	20.11	110	−13.22	2	[75]
Metal organic resin-2	3.725	3.64	13.56	/	/	/	/	/	/	3	[76]
Polytetraallylpropane diaminium	5.253	21.48	112.8	0.357	0.297	20	−7.042	52.401	−22.395	6	[53]
Polyelectrolytic hydrogels	0.790	2.132	1.684	0.612	0.322	30	/	/	/	6	[1]
Amine-magnetite nanoparticles	4.079	16.33	66.61	0.149	0.488	25	137.1	26.91	−3.28	3	[2]
L-Cysteine magnetite	0.663	215.3	142.7	2.512	0.293	45	73.31	280	−14.7	2	[10]
Ustilago maydis	2.530	0.300	0.759	2.4×10^{-2}	0.52	20	−9745	−38.685	856.54	2	[77]
Amine silica magnetite	3.561	/	/	/	/	Room	/	/	/	2	[57]
Nano- γ -Al_2O_3	0.267	101.4	27.07	0.318	0.161	25	/	/	/	3	[78]
Pteris vittata L.	3.206	1.56	5.001	1.179	0.27	30	21.0	200	−26.5	2	[59]
Chitosan magnetite	3.846	1.3	5.000	1.743	0.854	30	25.72	182	−29.4	3	[7]
Aspergillus niger	0.097	1142.3	110.8	2.14×10^{-3}	0.666	28	/	/	/	2.5	[37]
Mg_6AlFe-double hydroxide	3.385	0.0952	0.322	0.489	0.495	25	/	/	/	5	[79]
Alum-water treatment sludge	0.220	1.12	0.246	0.011	0.44	25	/	/	/	3	[18]
Palm kernel shell	0.955	113.7	108.6	0.0958	0.62	Room	/	/	/	6	[80]
Bacterial cellulose/ chitosan	2.925 *	/	/	/	/	25	/	/	/	6	[81]
Kaolinite nanotubes	4.579	0.143	0.655	0.0536	0.89	30	/	/	/	2	[82]
Bacterial cellulose/attapulgite	1.750	2.205	3.859	0.526	0.45	25	/	/	/	6	[83]
Char derived from South African coal	0.006	7.323	0.044	0.0096	0.665		/	/	/	2	[43]
Granular activated carbon	0.138	15.334	2.116	0.2433	0.611		/	/	/	7.5	[43]

* Experimental data.

3.3. Sorbent Affinity toward Cr(VI)

The sorbent affinity toward Cr(VI) can be evaluated from the Langmuir equilibrium constant (K_L): the higher K_L the higher the sorbent affinity for Cr(VI). Among tested sorbents (Table 1), *Sargassum bevanom* (K_L = 1160 L mmol^{-1}) [19] and *Aspergillus niger* (K_L = 1140 L mmol^{-1}) [37] exhibit the highest affinity for Cr(VI), followed by L-cysteine functionalized magnetite (K_L = 215 L mmol^{-1}) [10], magnetic ion exchange resin (K_L = 181 L mmol^{-1}) [38] and calcinated Al/Fe oxide–oxyhydroxide composite (K_L = 123 L mmol^{-1}) [67]. For practical purposes, it is also relevant to evaluate sorbent affinity at low Cr(VI) initial concentration. This parameter can be estimated from the initial slope of the Langmuir isotherm, which is the product of the maximum sorption capacity, q_m, and K_L. The highest values for Cr(VI) affinity at low Cr(VI) concentration have been reported for polypyrrole graphene oxide nanocomposite [62] and *Sargassum bevanom* [19] (see Table 1).

3.4. Sorption Thermodynamics

The change of sorption isotherms (i.e., of the equilibrium conditions) with temperature provides information on the temperature-dependence of the sorption equilibrium and related thermodynamic parameters, namely the standard change in Gibbs energy ($\Delta G°$), enthalpy ($\Delta H°$) and entropy ($\Delta S°$).

The temperature-dependence of the sorption equilibrium constant (K) is generally derived from the Gibbs-Helmholtz equation [84]:

$$\frac{\partial\left(\Delta G^{\circ}/T\right)}{\partial T} = -\frac{\Delta H^{\circ}}{T^2} \tag{21}$$

By using the well-known thermodynamic relationships:

$$\Delta G^{\circ} = -RTln(K) \tag{22}$$

$$\Delta G^{\circ} = \Delta H^{\circ} - T\Delta S^{\circ} \tag{23}$$

and assuming that neither $\Delta H°$ or $\Delta S°$ varies appreciably with temperature, Equation (21) can be integrated to give:

$$\ln(K) = -\frac{\Delta H^{\circ}}{R}\frac{1}{T} + \frac{\Delta S^{\circ}}{R} \tag{24}$$

A plot of ln$K$ vs. 1/T (van't Hoff plot) will produce a straight line whose slope and intercept with y-axis permit the determination of $\Delta H°$ and $\Delta S°$, respectively.

The value of K in Equation (24) depends on the model chosen for describing the sorption isotherm. The Langmuir equilibrium constant K_L is often used for this purpose in Cr(VI) sorption studies [35,51,75]; the sorption distribution coefficient $K_D = q_e/C_e$ (determined by extrapolating to zero the plot ln(q_e/C_e) against C_e) is also utilized, though less frequently [32,64,70].

Applying Equation (24), Kumar et al. [58] obtained positive values of $\Delta H°$, indicating that Cr(VI) sorption on zirconium oxide-immobilized alginate beads is an endothermic process. The same was reported by Dragan et al. [63] using anion exchanger microspheres embedded into chitosan/poly(vinyl amine), by Song et al. [68] using amine-functionalized magnetic corn stalk composites, and by many other authors (Table 1). Negative values of $\Delta H°$ are encountered less frequently in the literature, for example Gheju et al. [24] using MnO_2 and Albadarin et al. [51] using dolomite.

Crucially thermodynamic analyses of Cr(VI) sorption reported in the literature is often wrong [2,7,19,20,24,26,30,35,52,53,58,62,68,73,74,77]. The value of K (Equation (24)) has been erroneously determined on many occasions [2,7,20,24,30,52,53,58,62,68,73,77] using the following expression:

$$K = \frac{q_e}{C_e} \tag{25}$$

As easily inferred from any experimental isotherm curve (with the exception of linear isotherms), the q_e/C_e ratio is *not* constant (i.e., it varies with sorbent coverage [85]), thus Equation (25) does not

represent an equilibrium constant and cannot be used in the van't Hoff equation (Equation (24)). As already observed, a correct determination of K from the q_e/C_e ratio could be obtained by extrapolating its value at zero sorbent coverage [86–88].

For the same reasons, we consider incorrect the determination of K as:

$$K = \frac{F_e}{1 - F_e} \tag{26}$$

where F_e is the fraction of Cr(VI) sorbed at equilibrium [19,74].

Another mistake frequently observed in the literature concerns the meaning ascribed to the sign of ΔG°. Several authors [2,7,19,20,24,26,32,35,52,53,58,62,64,68,73] found a $\Delta G^\circ < 0$ and interpreted this as an indication of spontaneous Cr(VI) sorption. Others obtained a $\Delta G^\circ > 0$ and concluded that the instance of Cr(VI) sorption they examined was a non-spontaneous process [4,74,77]. These claims have been so long held that one tends to forget that the calculated change in Gibbs energy refers to *standard conditions*. A negative or positive ΔG° only indicates the spontaneity or non-spontaneity, respectively, of a *hypothetical* sorption process in which the reagents (sorbent and solute) and the product (adsorbent-solute adduct) are both in standard conditions [88]. The sign of ΔG° may even depend on the selected standard state [88,89]. It is worth remarking that the choice of the standard state not only influences the sign of ΔG° (hence the value of K [90]), but also the sign and magnitude of ΔS° (ΔH° is independent on the standard state because the ratio between K values at two different standard states is constant (see Equation (24)). From the above considerations, it follows that, for a correct comparison of thermodynamic parameters for sorption on different sorbents, these should be relative to similar standard conditions.

4. Kinetic Modelling

The study of sorption kinetics is of practical significance because it provides information on the time required for effective removal of a solute from the aqueous phase.

Among the models proposed for describing the kinetics of Cr(VI) sorption, the most popular ones are the pseudo-first order (PFO) and the pseudo-second order (PSO) model; other frequently used models are the Weber-Morris and the Elovich model.

The PFO model [91] assumes that the observed rate of sorption (dq/dt) is proportional to the distance from equilibrium expressed as the difference between the amount of Cr(VI) sorbed at equilibrium (q_e) and at any time (q):

$$\frac{dq}{dt} = k_{PFO}(q_e - q) \tag{27}$$

where k_{PFO} is the PFO kinetic rate constant. By integrating Equation (27) for the boundary conditions $t = 0$ to $t = t$ and $q = 0$ to $q = q$, we obtain:

$$q = q_e\left(1 - e^{-k_{PFO}t}\right) \tag{28}$$

The PSO model [92] differs from the PFO model because the sorption rate is assumed to be proportional to the square of the distance from equilibrium:

$$\frac{dq}{dt} = k_{PSO}(q_e - q)^2 \tag{29}$$

Here k_{PSO} is the PSO kinetic rate constant. Equation (29) can be integrated, for the same boundary conditions as for Equation (27), leading to:

$$q = \frac{{q_e}^2 k_{PSO} t}{1 + q_e k_{PSO} t} \tag{30}$$

It is widely maintained that the application of the PSO model to Cr(VI) sorption kinetic data gives better fitting results than the PFO model. Examples include studies carried out using as sorbent bacterial cellulose/attapulgite magnetic composites [83], palm oil kernel shell [80], cross linked-chitosan-grafted-polyaniline composite [64], teff straw [70] and material derived from harmful algal bloom biomass [27]. In contrast, Dragan et al. [63] found that the PFO model was best suited to describe the kinetic data of Cr(VI) sorption onto chitosan/poly(vinyl amine cryogel. Better applicability of the PFO model appears to be associated with weak Cr(VI)-sorbent interaction (physiosorption) [63], whereas better applicability of the PSO model is indicative of strong interaction (chemisorption) [41]. Noticeably, better performance of the PSO model may also be an artifact from improper analysis of the data. In most cases this results from the application of Equation (30) in the following linearized form [17,93]:

$$\frac{t}{q} = \frac{1}{k_{PSO}{q_e}^2} + \frac{t}{q_e} \tag{31}$$

According to Equation (31), if the data obey the pseudo-second order model, a plot of t/q vs. t should produce a straight line. The main drawback of this method is that for data points at (or very close to) equilibrium, the plot of t/q vs. t becomes linear independently of sorption kinetics [93]. The goodness of the results obtained by the plot of t/q vs. t may be verified by using a linearized form of the PSO model [17]:

$$\frac{q}{t} = k_{PSO}{q_e}^2 - k_{PSO}q_e q \tag{32}$$

If the PSO model is appropriate for the data, the plot of q/t against q will be linear. As an example, the comparison between t/q vs. t and q/t vs. q for the sorption of Cr(VI) onto MnO_2 [24] is reported in Figure 5. The authors claimed that the sorption kinetics was adequately described by the PSO model because the linear curve-fitting of t/q vs. t data gave excellent results (R^2 = 0.999, see Figure 5). However, as can be seen from Figure 5, this conclusion is incorrect because the same data, rearranged in the form q/t vs. q, significantly deviate from linearity.

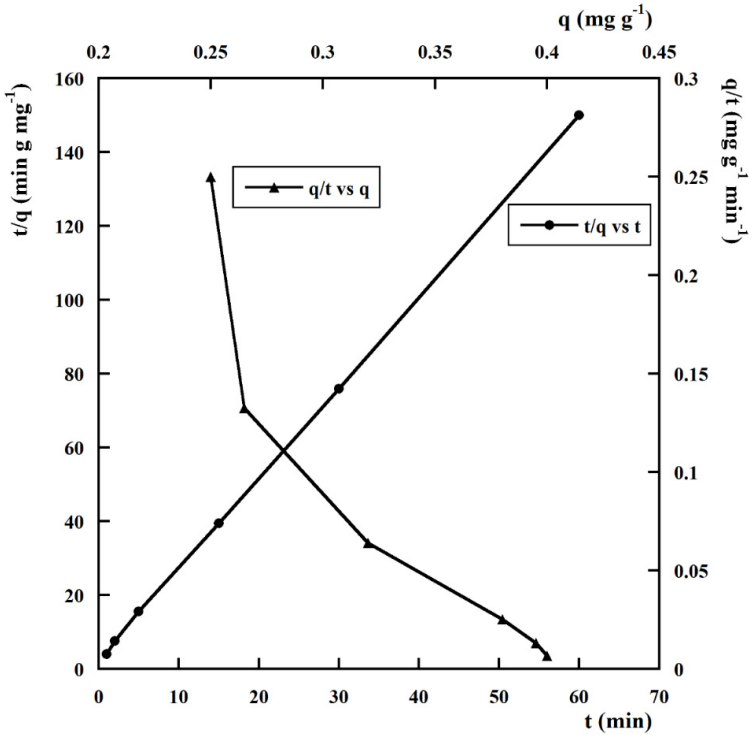

Figure 5. Comparison between the plots of q vs. t and q/t vs. q for the sorption of Cr(VI) onto MnO_2; initial Cr(VI) aqueous concentration = 0.02 mM, sorbent dosage = 2 g L^{-1}. Adapted from Gheju et al. [24].

As a general rule, the non-linear curve fitting is recommended over the linear curve fitting to prevent possible misinterpretation of the data. It is also worth observing that, because Cr(VI) sorption rate varies with operative conditions such as the initial solute concentration and the sorbent dosage, it is usually not possible to compare the values of k_{PFO} or k_{PSO} from different reports. To partially overcome this problem, one could, for example, compare the values of initial sorption rate (v_0) as predicted by the PFO and the PSO model, using Equations (33) and (34), respectively:

$$v_{0(PFO)} = k_{PFO} q_e \tag{33}$$

$$v_{0(PSO)} = k_{PSO} {q_e}^2 \tag{34}$$

Values of $v_{0(PFO)}$ and $v_{0(PSO)}$ from recent works are reported in Table 2. With very few exceptions [32,53], most of the studies report higher values of $v_{0(PSO)}$ compared to $v_{0(PFO)}$.

Table 2. Kinetic data for Cr(VI) sorption.

			PFO Model			PSO Model					
Sorbent Type	**C_0 (mmol L^{-1})**	**Sorbent Dosage (g L^{-1})**	**q_e (mmol g^{-1})**	**k_{PFO} (h^{-1})**	**$v_{0(PFO)}$ (mmol g^{-1} h^{-1})**	**q_e (mmol g^{-1})**	**k_{PSO} (g $mmol^{-1}$ h^{-1})**	**$v_{0(PSO)}$ (mmol g^{-1} h^{-1})**	**T (°C)**	**pH**	**Ref.**
Magnetic ion exchange resin	1.00	1	0.77	9.6	7.392	0.81	29.4	19.29	25	4	[38]
Zero-valent iron-carboxymethyl cellulose	1.92	0.75	1.648	0.78	1.285	1.629	0.822	2.181	25	5.6	[41]
Zirconium oxide-alginate beads	0.365	2.5	0.0409	0.0624	2.552×10^{-3}	0.0388	3.156	4.751×10^{-3}	25	5	[58]
Mg–Al hydrotalcite	3.85	2	1.471	9.9	14.56	1.468	9.36	20.17	Room	6	[35]
Anion exchanger chitosan/poly(vinyl amine)	1.92	1.25	1.482	1.112	1.648	1.595	1.091	2.775	25	5.5	[63]
Cross linked-chitosan-polyaniline	7.69	2	/	10.44		3.293	12.43	134.8	30	4.2	[64]
Mg-Zn-Al hydrotalcite derived oxides	0.192	5	0.886	2.1	1.861	1.147	1.751	2.304	30	6	[65]
Fe (II)-modified natural zeolite	2.88	200	/	/	/	0.0157	700	0.0173	Room	5.5	[66]
Anion-exchange resins	1.92	1.67	0.0577	3.624	0.209	/	/	/	27	5	[20]
MnO_2	0.04	2	8.07×10^{-3}	3.72	0.0300	0.0102	5678.4	0.591	20	6.9	[24]
Iron/carbon Fe/C composites	1.92	1	0.628	0.0074	4.647×10^{-3}	0.836	0.0392	0.0328	Room	5	[27]
Cereal by-product carbon	2.54	2	8.358×10^{-3}	0.120	1.00×10^{-3}	0.149	13.55×10^{5}	30.08×10^{4}	20	6	[4]
Amine-functionalized corn stalk	3.85	1	2142.4	0.462	989.8	3.698	134.16	1834.7	45	3	[68]
Dolomite	0.961	1	0.194	0.0452	8.769×10^{-3}	0.249	0.179	0.011	20	2	[51]
Acinetobacter junii VITSUKMW2	1.92	2	0.202	1.08	0.218	0.492	12.48	3.021	27	2	[48]
Polypyrrole graphene oxide	1.92	0.5	5.215	2.136	11.14	3.846	6.24	92.30	25	2	[62]
Sargassum bevanom	1.92	7	/	/	/	0.274	16.91	1.269	20	3	[19]
Iron oxide-activated carbon	0.961	5	5.96×10^{-3}	6.36	0.0380	0.0460	6895.2	14.59	25	2	[49]
Chitosan-xylan–TiO_2	1.92	5	1.760	0.593	1.044	1.273	0.551	0.893	45	7	[32]
Teff straw	1.92	10	0.137	1.68	0.230	0.175	15.6	0.478	45	2	[70]
Codium tomentosum		10	/	/	/	/	/	/	20	2	[54]
β-Cyclodextrin-polyurethane	0.0192	0.2	/	/	/	4.638×10^{-3}	884	0.0190	25	3	[72]
Resin Tulsion A-27	1.1	0.833	1.1	1.724	1.90	/	/	/	50	5.5	[30]
Solid biodiesel waste residue	9.61	6	0.531	1.02	0.542	2.404	4.642	26.83	30	2	[73]
Pediastrum boryanum	7.69	4	0.329	2.73	0.898	0.581	748.8	252.8	25	2	[26]
Trewia nudiflora	2.15	0.75	0.433	1.68	0.727	2.709	13.01	95.48	30	2	[75]
Alum-water treatment sludge	0.001	10	0.027	0.564	0.0152	0.079	58.02	0.362	25	3	[18]
Polytetra-allylpropane diaminium	1.92	0.7	2.612	18.80	49.10	0.0521	16.55	0.0449	20	6	[53]
Amine-magnetite nanoparticles	0.096	1	0.123	3.6	0.443	0.543	6.24	1.840	25	3	[2]
Ustilago maydis	0.48	10	/	/		0.0375	42.74	0.0601	20	5.5	[77]
Amine silica magnetite	2.88	1.07	0.631	19.92	12.57	2.497	205.3	1280	Room	2	[57]
Nano-γ-Al_2O_3	0.38	3	0.011	1.2	0.0132	0.156	93.6	2.278	25	3	[78]
Pteris vittata L.	1.92	1	/	/	/	1.479	3.12	6.825	30	2	[59]
Aspergillus niger	0.96	10	8.32×10^{-3}	0.054	4.493×10^{-4}	8.30×10^{-3}	17,238	1.187	28	2.5	[37]
Palm kernel shell	0.096	20	/	/	/	/	$1.2 \times 10\text{-}^{5}$	/	Room	6	[80]
Bacterial cellulose/chitosan			/	/	/	/	/	/	25	6	[81]
Kaolinite nanotubes	1.92	0.333	/	/	/	1.074	4.802	5.534	30	2	[82]
Bacterial cellulose/attapulgite	0.96	0.2	1.473	56.7	83.52	1.635	3.25×10^{6}	8.688×10^{6}	25	6	[83]

The Weber-Morris equation [94] is a semi-empirical model often used in Cr(VI) sorption studies for evaluating whether the rate of the process is affected by solute diffusion within sorbent pores (intra-particle diffusion):

$$q = k_D \sqrt{t} + \kappa \tag{35}$$

Here k_D is a kinetic diffusion parameter and κ is a constant proportional to the thickness of the diffusion boundary layer. A linear correlation between q and the root square of time suggests that the rate of Cr(VI) sorption is controlled by diffusion [19,32,73]. Some authors argued that the presence of multiple linear portions in the q vs. $\sqrt{t}$ plot indicates that the sorption process proceeds through two or more consecutive diffusive steps [75].

Another model used for modelling the sorption kinetic data is the Elovich equation [95], which envisages an exponential decrease of the sorption rate with an increase of bound sorbate q, without reaching equilibrium (for $t \to \infty$, $q \to \infty$):

$$\frac{dq}{dt} = \alpha e^{-\beta q} \tag{36}$$

where α is the initial ($t = 0$) sorption rate and β indicates the extent to which the rate varies with q. It is agreed that the applicability of the Elovich model to experimental data provides evidence of heterogeneity of sorption sites [75]. Equation (36) can be integrated for the boundary conditions $t = 0$ to $t = t$ and $q = 0$ to $q = q$, yielding:

$$q = \frac{1}{\beta} \ln(1 + \alpha\beta t) \tag{37}$$

Owing to historical difficulties (lack of computational power) associated with the application of non-linear curve fitting [96], an *approximated*-linearized form of Equation (37) was introduced by Chien and Clayton [97] for testing the applicability of the Elovich model. The approximated form of the integrated Elovich equation was derived on the assumption that for sufficiently high values of t, the term $\alpha \cdot \beta \cdot t$ becomes much greater than 1 so that Equation (37) reduces to:

$$q = \frac{1}{\beta} \ln \alpha\beta + \ln t \tag{38}$$

Thus, the validity of Equation (38) is verified by the linear plot of q vs. $\ln t$. Although non-linear curve fitting is now easy to perform, linearization is still the first-choice procedure for testing the Elovich model, which may lead to incorrect interpretation of data. As a matter of fact, several recent studies of Cr(VI) sorption reported that the linearized Elovich equation (Equation (38)) gave less satisfactory fitting results than the PSO model [4,19,75,82]. However, as stated above, the exact integrated form for the Elovich equation (Equation (37)) ought to be employed for a rigorous comparison with the PSO model.

5. Conclusions

The primary mechanism of chromium sorption involves electrostatic interactions between the sorbate and the sorbent surface. The pH strongly affects chromium sorption behavior. The most frequently used models to describe the equilibrium of Cr(VI) sorption are the Langmuir model and the Freundlich model, the former usually providing better fitting results. The Pseudo First-Order and the Pseudo Second-Order model are the models of choice for the kinetics of Cr(VI) sorption. The Pseudo Second-Order model generally fits the data much better than the Pseudo First-Order model.

A critical survey shows that thermodynamic and kinetic analyses of Cr(VI) sorption reported in the recent literature are often incorrect. Common mistakes include miscalculation of the sorption equilibrium constant, erroneous extrapolation of data to standard conditions, and the application of regression models in linearized form.

Author Contributions: Conceptualization, S.S.; data curation, P.I. and A.F.; writing—original draft preparation, A.F. and S.S.; writing—review and editing, S.C. and S.S.; supervision, D.M. and S.S. All authors have read and agreed to the published version of the manuscript.

Funding: This research has been supported by VALERE "VAnviteLli pEr la RicErca" PROGRAMME funded by the University of Campania "Luigi Vanvitelli".

Acknowledgments: The authors are grateful to Roberto Ligrone for very useful comments and suggestions.

Conflicts of Interest: The authors declare no conflict of interest.

References

1. Roy, P.K.; Swami, V.; Kumar, D.; Rajagopal, C. Removal of toxic metals using superabsorbent polyelectrolytic hydrogels. *J. Appl. Polym. Sci.* **2011**, *122*, 2415–2423. [CrossRef]
2. Norouzian Baghani, A.; Mahvi, A.H.; Gholami, M.; Rastkari, N.; Delikhoon, M. One-Pot synthesis, characterization and adsorption studies of amine-functionalized magnetite nanoparticles for removal of Cr (VI) and Ni (II) ions from aqueous solution: Kinetic, isotherm and thermodynamic studies. *J. Environ. Health Sci. Eng.* **2016**, *14*. [CrossRef]
3. Johnston, C.P.; Chrysochoou, M. Mechanisms of chromate adsorption on hematite. *Geochim. Cosmochim. Acta* **2014**, *138*, 146–157. [CrossRef]
4. Arris, S.; Bencheikh Lehocine, M.; Meniai, A.H. Sorption study of chromium sorption from wastewater using cereal by-products. *Int. J. Hydrog. Energy* **2016**, *41*, 10299–10310.
5. Kowalski, Z. Treatment of chromic tannery wastes. *J. Hazard. Mater.* **1994**, *37*, 137–141. [CrossRef]
6. Janoš, P.; Hůla, V.; Bradnová, P.; Pilařová, V.; Šedlbauer, J. Reduction and immobilization of hexavalent chromium with coal- and humate-based sorbents. *Chemosphere* **2009**, *75*, 732–738. [CrossRef] [PubMed]
7. Tran, H.V.; Tran, T.L.; Le, T.D.; Le, T.D.; Nguyen, H.M.T.; Dang, L.T. Graphene oxide enhanced adsorption capacity of chitosan/magnetite nanocomposite for Cr(VI) removal from aqueous solution. *Mater. Res. Express* **2019**, *6*, 025018. [CrossRef]
8. Mikhaylov, V.I.; Maslennikova, T.P.; Krivoshapkina, E.F.; Tropnikov, E.M.; Krivoshapkin, P.V. Express Al/Fe oxide–oxyhydroxide sorbent systems for Cr(VI) removal from aqueous solutions. *Chem. Eng. J.* **2018**, *350*, 344–355. [CrossRef]
9. Shi, X.; Dalal, N.S. On the hydroxyl radical formation in the reaction between hydrogen peroxide and biologically generated chromium(V) species. *Arch. Biochem. Biophys.* **1990**, *277*, 342–350. [CrossRef]
10. Bagbi, Y.; Sarswat, A.; Mohan, D.; Pandey, A.; Solanki, P.R. Lead and Chromium Adsorption from Water using L-Cysteine Functionalized Magnetite (Fe3O4) Nanoparticles. *Sci. Rep.* **2017**, *7*. [CrossRef]
11. Huang, C.P.; Wu, M.H. Chromium removal by carbon adsorption. *J. Water Pollut. Control Fed.* **1975**, *47*, 2437–2446.
12. Huang, C.P.; Wu, M.H. The removal of chromium(VI) from dilute aqueous solution by activated carbon. *Water Res.* **1977**, *11*, 673–679. [CrossRef]
13. Hamadi, N.K.; Chen, X.D.; Farid, M.M.; Lu, M.G.Q. Adsorption kinetics for the removal of chromium(VI) from aqueous solution by adsorbents derived from used tyres and sawdust. *Chem. Eng. J.* **2001**, *84*, 95–105. [CrossRef]
14. Khan, S.A.; Riaz-ur-Rehman Khan, M.A. Adsorption of chromium (III), chromium (VI) and silver (I) on bentonite. *Waste Manag.* **1995**, *15*, 271–282. [CrossRef]
15. Sharma, D.C.; Forster, C.F. A preliminary examination into the adsorption of hexavalent chromium using low-cost adsorbents. *Bioresour. Technol.* **1994**, *47*, 257–264. [CrossRef]
16. Sharma, D.C.; Forster, C.F. Removal of hexavalent chromium using sphagnum moss peat. *Water Res.* **1993**, *27*, 1201–1208. [CrossRef]
17. Salvestrini, S.; Vanore, P.; Bogush, A.; Mayadevi, S.; Campos, L.C. Sorption of metaldehyde using granular activated carbon. *J. Water Reuse Desalin.* **2017**, *7*, 280–287. [CrossRef]
18. Zhou, Y.F.; Haynes, R.J. Removal of Pb(II), Cr(III) and Cr(VI) from aqueous solutions using alum-derived water treatment sludge. *Water. Air. Soil Pollut.* **2011**, *215*, 631–643. [CrossRef]
19. Javadian, H.; Ahmadi, M.; Ghiasvand, M.; Kahrizi, S.; Katal, R. Removal of Cr(VI) by modified brown algae Sargassum bevanom from aqueous solution and industrial wastewater. *J. Taiwan Inst. Chem. Eng.* **2013**, *44*, 977–989. [CrossRef]

20. Shi, T.; Wang, Z.; Liu, Y.; Jia, S.; Changming, D. Removal of hexavalent chromium from aqueous solutions by D301, D314 and D354 anion-exchange resins. *J. Hazard. Mater.* **2009**, *161*, 900–906. [CrossRef]
21. Das, S.K.; Guha, A.K. Biosorption of hexavalent chromium by Termitomyces clypeatus biomass: Kinetics and transmission electron microscopic study. *J. Hazard. Mater.* **2009**, *167*, 685–691. [CrossRef] [PubMed]
22. Kantar, C.; Ari, C.; Keskin, S.; Dogaroglu, Z.G.; Karadeniz, A.; Alten, A. Cr(VI) removal from aqueous systems using pyrite as the reducing agent: Batch, spectroscopic and column experiments. *J. Contam. Hydrol.* **2015**, *174*, 28–38. [CrossRef] [PubMed]
23. Gherasim, C.V.; Bourceanu, G.; Olariu, R.I.; Arsene, C. A novel polymer inclusion membrane applied in chromium (VI) separation from aqueous solutions. *J. Hazard. Mater.* **2011**, *197*, 244–253. [CrossRef]
24. Gheju, M.; Balcu, I.; Mosoarca, G. Removal of Cr(VI) from aqueous solutions by adsorption on MnO2. *J. Hazard. Mater.* **2016**, *310*, 270–277. [CrossRef] [PubMed]
25. Kyzas, G.Z.; Kostoglou, M.; Lazaridis, N.K. Copper and chromium(VI) removal by chitosan derivatives-Equilibrium and kinetic studies. *Chem. Eng. J.* **2009**, *152*, 440–448. [CrossRef]
26. Ozer, T.B.; Erkaya, I.A.; Udoh, A.U.; Duygu, D.Y.; Akbulut, A.; Bayramoglu, G.; Arica, M.Y. Biosorption of Cr(VI) by free and immobilized Pediastrum boryanum biomass: Equilibrium, kinetic, and thermodynamic studies. *Environ. Sci. Pollut. Res.* **2012**, *19*, 2983–2993. [CrossRef]
27. Cui, Y.; Masud, A.; Aich, N.; Atkinson, J.D. Phenol and Cr(VI) removal using materials derived from harmful algal bloom biomass: Characterization and performance assessment for a biosorbent, a porous carbon, and Fe/C composites. *J. Hazard. Mater.* **2019**, *368*, 477–486. [CrossRef]
28. Campos, V. The sorption of toxic elements onto natural zeolite, synthetic goethite and modified powdered block carbon. *Environ. Earth Sci.* **2009**, *59*, 737–744. [CrossRef]
29. Di Natale, F.; Erto, A.; Lancia, A.; Musmarra, D. Equilibrium and dynamic study on hexavalent chromium adsorption onto activated carbon. *J. Hazard. Mater.* **2015**, *281*, 47–55. [CrossRef]
30. Koujalagi, P.S.; Divekar, S.V.; Kulkarni, R.M.; Nagarale, R.K. Kinetics, thermodynamic, and adsorption studies on removal of chromium(VI) using Tulsion A-27(MP) resin. *Desalin. Water Treat.* **2013**, *51*, 3273–3283. [CrossRef]
31. Chakravarty, R.; Khan, M.M.R.; Das, A.R.; Guha, A.K. Biosorptive removal of chromium by husk of Lathyrus sativus: Evaluation of the binding mechanism, kinetic and equilibrium study. *Eng. Life Sci.* **2013**, *13*, 312–322. [CrossRef]
32. Wu, S.; Hu, J.; Wei, L.; Du, Y.; Shi, X.; Deng, H.; Zhang, L. Construction of porous chitosan-xylan-TiO2 hybrid with highly efficient sorption capability on heavy metals. *J. Environ. Chem. Eng.* **2014**, *2*, 1568–1577. [CrossRef]
33. Salvestrini, S.; Sagliano, P.; Iovino, P.; Capasso, S.; Colella, C. Atrazine adsorption by acid-activated zeolite-rich tuffs. *Appl. Clay Sci.* **2010**, *49*, 330–335. [CrossRef]
34. González, P.S.; Ambrosio, L.F.; Paisio, C.E.; Talano, M.A.; Medina, M.I.; Agostini, E. Chromium (VI) remediation by a native strain: Effect of environmental conditions and removal mechanisms involved. *Environ. Sci. Pollut. Res.* **2014**, *21*, 13551–13559. [CrossRef]
35. Khitous, M.; Salem, Z.; Halliche, D. Effect of interlayer anions on chromium removal using Mg-Al layered double hydroxides: Kinetic, equilibrium and thermodynamic studies. *Chin. J. Chem. Eng.* **2016**, *24*, 433–445. [CrossRef]
36. Mahmoud, M.E.; Yakout, A.A.; Abdel-Aal, H.; Osman, M.M. Speciation and selective biosorption of Cr(III) and Cr(VI) using nanosilica immobilized-fungi biosorbents. *J. Environ. Eng.* **2015**, *141*. [CrossRef]
37. Do Vale, M.S.; do Nascimento, R.F.; Leitão, R.C.; Santaella, S.T. Cr and Zn biosorption by Aspergillus niger. *Environ. Earth Sci.* **2016**, *75*. [CrossRef]
38. Hans, R.; Senanayake, G.; Dharmasiri, L.C.S.; Mathes, J.A.P.; Kim, D.J. A preliminary batch study of sorption kinetics of Cr(VI) ions from aqueous solutions by a magnetic ion exchange (MIEX®) resin and determination of film/pore diffusivity. *Hydrometallurgy* **2016**, *164*, 208–218. [CrossRef]
39. Bibi, I.; Niazi, N.K.; Choppala, G.; Burton, E.D. Chromium(VI) removal by siderite ($FeCO_3$) in anoxic aqueous solutions: An X-ray absorption spectroscopy investigation. *Sci. Total Environ.* **2018**, *640–641*, 1424–1431. [CrossRef]
40. Zhang, Z.; Guo, G.; Li, X.; Zhao, Q.; Bi, X.; Wu, K.; Chen, H. Effects of hydrogen-peroxide supply rate on schwertmannite microstructure and chromium(VI) adsorption performance. *J. Hazard. Mater.* **2019**, *367*, 520–528. [CrossRef]

41. Zhang, S.; Lyu, H.; Tang, J.; Song, B.; Zhen, M.; Liu, X. A novel biochar supported CMC stabilized nano zero-valent iron composite for hexavalent chromium removal from water. *Chemosphere* **2019**, *217*, 686–694. [CrossRef] [PubMed]
42. Erto, A.; Andreozzi, R.; Di Natale, F.; Lancia, A.; Musmarra, D. Experimental and isotherm-models analysis on TCE and PCE adsorption onto activated carbon. *Chem. Eng. Trans.* **2009**, *17*, 293–298. [CrossRef]
43. Di Natale, F.; Lancia, A.; Molino, A.; Musmarra, D. Removal of chromium ions form aqueous solutions by adsorption on activated carbon and char. *J. Hazard. Mater.* **2007**, *145*, 381–390. [CrossRef]
44. Langmuir, I. The adsorption of gases on plane surfaces of glass, mica and platinum. *J. Am. Chem. Soc.* **1918**, *40*, 1361–1403. [CrossRef]
45. Salvestrini, S. Analysis of the Langmuir rate equation in its differential and integrated form for adsorption processes and a comparison with the pseudo first and pseudo second order models. *React. Kinet. Mech. Catal.* **2018**, *123*, 455–472. [CrossRef]
46. Salvestrini, S. A modification of the Langmuir rate equation for diffusion-controlled adsorption kinetics. *React. Kinet. Mech. Catal.* **2019**, *128*, 571–586. [CrossRef]
47. Freundlich, H. Über die Adsorption in Lösungen. *Z. Phys. Chem.* **2017**, *57*, 385–470. [CrossRef]
48. Paul, M.L.; Samuel, J.; Chandrasekaran, N.; Mukherjee, A. Comparative kinetics, equilibrium, thermodynamic and mechanistic studies on biosorption of hexavalent chromium by live and heat killed biomass of Acinetobacter junii VITSUKMW2, an indigenous chromite mine isolate. *Chem. Eng. J.* **2012**, *187*, 104–113. [CrossRef]
49. Jain, M.; Yadav, M.; Kohout, T.; Lahtinen, M.; Garg, V.K.; Sillanpää, M. Development of iron oxide/activated carbon nanoparticle composite for the removal of Cr(VI), Cu(II) and Cd(II) ions from aqueous solution. *Water Resour. Ind.* **2018**, *20*, 54–74. [CrossRef]
50. Kim, E.J.; Park, S.; Hong, H.J.; Choi, Y.E.; Yang, J.W. Biosorption of chromium (Cr(III)/Cr(VI)) on the residual microalga Nannochloris oculata after lipid extraction for biodiesel production. *Bioresour. Technol.* **2011**, *102*, 11155–11160. [CrossRef]
51. Albadarin, A.B.; Mangwandi, C.; Al-Muhtaseb, A.H.; Walker, G.M.; Allen, S.J.; Ahmad, M.N.M. Kinetic and thermodynamics of chromium ions adsorption onto low-cost dolomite adsorbent. *Chem. Eng. J.* **2012**, *179*, 193–202. [CrossRef]
52. Sirusbakht, S.; Vafajoo, L.; Soltani, S.; Habibi, S. Sawdust bio sorption of chromium (VI) ions from aqueous solutions. *Chem. Eng. Trans.* **2018**, *70*, 1147–1152. [CrossRef]
53. Liu, L.; Yang, Z.; Zhao, L.; Liu, J.; Liu, X.; Xue, J.; Tang, A. Removal performance and mechanism of poly(N1,N1,N3,N3-tetraallylpropane-1,3-diaminium chloride) toward Cr(VI). *Environ. Technol.* **2020**, *41*, 2450–2463. [CrossRef] [PubMed]
54. Anandaraj, B.; Eswaramoorthi, S.; Rajesh, T.P.; Aravind, J.; Suresh Babu, P. Chromium(VI) adsorption by Codium tomentosum: Evidence for adsorption by porous media from sigmoidal dose–response curve. *Int. J. Environ. Sci. Technol.* **2018**, *15*, 2595–2606. [CrossRef]
55. Sutkowy, M.; Klosowski, G. Use of the coenobial green algae Pseudopediastrum boryanum (Chlorophyceae) to remove hexavalent chromium from contaminated aquatic ecosystems and industrialwastewaters. *Water* **2018**, *10*, 712. [CrossRef]
56. Jemima, W.S.; Magesan, P.; Chiranjeevi, P.; Umapathy, M.J. Sorption Properties of Organo Modified Montmorillonite Clay for the Reclamation of Chromium (VI) from Waste Water. *Silicon* **2019**, *11*, 925–933. [CrossRef]
57. Shariati, S.; Khabazipour, M.; Safa, F. Synthesis and application of amine functionalized silica mesoporous magnetite nanoparticles for removal of chromium(VI) from aqueous solutions. *J. Porous Mater.* **2017**, *24*, 129–139. [CrossRef]
58. Kumar, R.; Kim, S.J.; Kim, K.H.; Lee, S.H.; Park, H.S.; Jeon, B.H. Removal of hazardous hexavalent chromium from aqueous phase using zirconium oxide-immobilized alginate beads. *Appl. Geochem.* **2018**, *88*, 113–121. [CrossRef]
59. Prabhu, S.G.; Srinikethan, G.; Hegde, S. Spontaneous Cr(VI) and Cd(II) biosorption potential of native pinnae tissue of Pteris vittata L., a tropical invasive pteridophyte. *Int. J. Phytoremediat.* **2019**, *21*, 380–390. [CrossRef] [PubMed]
60. Sun, X.F.; Liu, C.; Ma, Y.; Wang, S.G.; Gao, B.Y.; Li, X.M. Enhanced Cu(II) and Cr(VI) biosorption capacity on poly(ethylenimine) grafted aerobic granular sludge. *Colloids Surf. B Biointerfaces* **2011**, *82*, 456–462. [CrossRef]

61. Sips, R. On the structure of a catalyst surface. II. *J. Chem. Phys.* **1950**, *18*, 1024–1026. [CrossRef]
62. Setshedi, K.Z.; Bhaumik, M.; Onyango, M.S.; Maity, A. High-performance towards Cr(VI) removal using multi-active sites of polypyrrole-graphene oxide nanocomposites: Batch and column studies. *Chem. Eng. J.* **2015**, *262*, 921–931. [CrossRef]
63. Dragan, E.S.; Humelnicu, D.; Dinu, M.V.; Olariu, R.I. Kinetics, equilibrium modeling, and thermodynamics on removal of Cr(VI) ions from aqueous solution using novel composites with strong base anion exchanger microspheres embedded into chitosan/poly(vinyl amine) cryogels. *Chem. Eng. J.* **2017**, *330*, 675–691. [CrossRef]
64. Karthik, R.; Meenakshi, S. Facile synthesis of cross linked-chitosan-grafted-polyaniline composite and its Cr(VI) uptake studies. *Int. J. Biol. Macromol.* **2014**, *67*, 210–219. [CrossRef] [PubMed]
65. Dudek, B.; Kuśtrowski, P.; Bialas, A.; Natkański, P.; Piwowarska, Z.; Chmielarz, L.; Kozak, M.; Michalik, M. Influence of textural and structural properties of Mg Al and Mg Zn Al containing hydrotalcite derived oxides on Cr(VI) adsorption capacity. *Mater. Chem. Phys.* **2012**, *132*, 929–936. [CrossRef]
66. Lv, G.; Li, Z.; Jiang, W.T.; Ackley, C.; Fenske, N.; Demarco, N. Removal of Cr(VI) from water using Fe(II)-modified natural zeolite. *Chem. Eng. Res. Des.* **2014**, *92*, 384–390. [CrossRef]
67. Mikhaylov, V.I.; Maslennikova, T.P.; Ugolkov, V.L.; Krivoshapkin, P.V. Hydrothermal synthesis, characterization and sorption properties of Al/Fe oxide-oxyhydroxide composite powders. *Adv. Powder Technol.* **2016**, *27*, 756–764. [CrossRef]
68. Song, W.; Gao, B.; Zhang, T.; Xu, X.; Huang, X.; Yu, H.; Yue, Q. High-capacity adsorption of dissolved hexavalent chromium using amine-functionalized magnetic corn stalk composites. *Bioresour. Technol.* **2015**, *190*, 550–557. [CrossRef]
69. Sreenivas, K.M.; Inarkar, M.B.; Gokhale, S.V.; Lele, S.S. Re-utilization of ash gourd (*Benincasa hispida*) peel waste for chromium (VI) biosorption: Equilibrium and column studies. *J. Environ. Chem. Eng.* **2014**, *2*, 455–462. [CrossRef]
70. Wassie, A.B.; Srivastava, V.C. Teff straw characterization and utilization for chromium removal from wastewater: Kinetics, isotherm and thermodynamic modelling. *J. Environ. Chem. Eng.* **2016**, *4*, 1117–1125. [CrossRef]
71. Arcos-Casarrubias, J.A.; Cruz-Díaz, M.R.; Cardoso-Martínez, J.; Vázquez-Arenas, J.; Caballero-Domínguez, F.V. Chromium adsorption into a macroporous resin based on vinylpyridine–divinylbenzene copolymers: Thermodynamics, kinetics, and process dynamic in a fixed bed column. *Adsorption* **2018**, *24*, 105–120. [CrossRef]
72. Badruddoza, A.Z.M.; Bhattarai, B.; Suri, R.P.S. Environmentally Friendly β-Cyclodextrin-Ionic Liquid Polyurethane-Modified Magnetic Sorbent for the Removal of PFOA, PFOS, and Cr(VI) from Water. *ACS Sustain. Chem. Eng.* **2017**, *5*, 9223–9232. [CrossRef]
73. Muthusamy, S.; Venkatachalam, S.; Jeevamani, P.M.K.; Rajarathinam, N. Biosorption of Cr(VI) and Zn(II) ions from aqueous solution onto the solid biodiesel waste residue: Mechanistic, kinetic and thermodynamic studies. *Environ. Sci. Pollut. Res.* **2014**, *21*, 593–608. [CrossRef]
74. Olguín, M.T.; López-González, H.; Serrano-Gómez, J. Hexavalent chromium removal from aqueous solutions by Fe-modified peanut husk. *Water. Air. Soil Pollut.* **2013**, *224*. [CrossRef]
75. Bhattacharya, P.; Banerjee, P.; Mallick, K.; Ghosh, S.; Majumdar, S.; Mukhopadhyay, A.; Bandyopadhyay, S. Potential of biosorbent developed from fruit peel of Trewia nudiflora for removal of hexavalent chromium from synthetic and industrial effluent: Analyzing phytotoxicity in germinating Vigna seeds. *J. Environ. Sci. Health Part A Toxic/Hazard. Subst. Environ. Eng.* **2013**, *48*, 706–719. [CrossRef]
76. Rapti, S.; Sarma, D.; Diamantis, S.A.; Skliri, E.; Armatas, G.S.; Tsipis, A.C.; Hassan, Y.S.; Alkordi, M.; Malliakas, C.D.; Kanatzidis, M.G.; et al. All in one porous material: Exceptional sorption and selective sensing of hexavalent chromium by using a Zr^{4+} MOF. *J. Mater. Chem. A* **2017**, *5*, 14707–14719. [CrossRef]
77. Serrano-Gómez, J.; Olguín, M.T. Separation of Cr(VI) from aqueous solutions by adsorption on the microfungus Ustilago maydis. *Int. J. Environ. Sci. Technol.* **2015**, *12*, 2559–2566. [CrossRef]
78. Shokati Poursani, A.; Nilchi, A.; Hassani, A.H.; Shariat, M.; Nouri, J. A novel method for synthesis of nano-γ-Al_2O_3: Study of adsorption behavior of chromium, nickel, cadmium and lead ions. *Int. J. Environ. Sci. Technol.* **2015**, *12*, 2003–2014. [CrossRef]
79. Zhang, F.; Du, N.; Li, H.; Song, S.; Hou, W. Sorbent effect on the sorption of Cr(VI) on a Mg6AlFe-layered double hydroxide and its calcined product in aqueous solutions. *Colloid Polym. Sci.* **2015**, *293*, 1961–1969. [CrossRef]

80. Baby, R.; Saifullah, B.; Hussein, M.Z. Palm Kernel Shell as an effective adsorbent for the treatment of heavy metal contaminated water. *Sci. Rep.* **2019**, *9*. [CrossRef] [PubMed]
81. Li, D.; Tian, X.; Wang, Z.; Guan, Z.; Li, X.; Qiao, H.; Ke, H.; Luo, L.; Wei, Q. Multifunctional adsorbent based on metal-organic framework modified bacterial cellulose/chitosan composite aerogel for high efficient removal of heavy metal ion and organic pollutant. *Chem. Eng. J.* **2020**, *383*. [CrossRef]
82. Abukhadra, M.R.; Bakry, B.M.; Adlii, A.; Yakout, S.M.; El-Zaidy, M.A. Facile conversion of kaolinite into clay nanotubes (KNTs) of enhanced adsorption properties for toxic heavy metals (Zn^{2+}, Cd^{2+}, Pb^{2+}, and Cr^{6+}) from water. *J. Hazard. Mater.* **2019**, *374*, 296–308. [CrossRef] [PubMed]
83. Chen, X.; Cui, J.; Xu, X.; Sun, B.; Zhang, L.; Dong, W.; Chen, C.; Sun, D. Bacterial cellulose/attapulgite magnetic composites as an efficient adsorbent for heavy metal ions and dye treatment. *Carbohydr. Polym.* **2020**, *229*. [CrossRef]
84. Atkins, P.; de Paula, J.; Keeler, J. *Atkins' Physical Chemistry*; OUP Oxford: Oxford, UK, 2017; ISBN 978-0198769866.
85. Fenti, A.; Iovino, P.; Salvestrini, S. Some remarks on "A critical review of the estimation of the thermodynamic parameters on adsorption equilibria. Wrong use of equilibrium constant in the Van't Hoof equation for calculation of thermodynamic parameters of adsorption". *J. Mol. Liq.* **2019**, *276*, 529–530. [CrossRef]
86. Khan, A.A.; Singh, R.P. Adsorption thermodynamics of carbofuran on Sn (IV) arsenosilicate in H^+, Na^+ and Ca^{2+} forms. *Colloids Surf.* **1987**, *24*, 33–42. [CrossRef]
87. Chianese, S.; Fenti, A.; Iovino, P.; Musmarra, D.; Salvestrini, S. Sorption of organic pollutants by humic acids: A review. *Molecules* **2020**, *25*, 918. [CrossRef]
88. Salvestrini, S.; Leone, V.; Iovino, P.; Canzano, S.; Capasso, S. Considerations about the correct evaluation of sorption thermodynamic parameters from equilibrium isotherms. *J. Chem. Thermodyn.* **2014**, *68*, 310–316. [CrossRef]
89. Salvestrini, S.; Fenti, A.; Chianese, S.; Iovino, P.; Musmarra, D. Diclofenac sorption from synthetic water: Kinetic and thermodynamic analysis. *J. Environ. Chem. Eng.* **2020**, *8*, 104105. [CrossRef]
90. Canzano, S.; Iovino, P.; Salvestrini, S.; Capasso, S. Comment on "Removal of anionic dye Congo red from aqueous solution by raw pine and acid-treated pine cone powder as adsorbent: Equilibrium, thermodynamic, kinetics, mechanism and process design". *Water Res.* **2012**, *46*, 4314–4315. [CrossRef]
91. Lagergren, S.K. About the theory of so-called adsorption of soluble substances, Kungliga Svenska Vetenskapsakademiens. *Handl. Band* **1898**, *24*, 1.
92. Ho, Y.S.; McKay, G. Pseudo-second order model for sorption processes. *Process Biochem.* **1999**, *34*, 451–465. [CrossRef]
93. Canzano, S.; Iovino, P.; Leone, V.; Salvestrini, S.; Capasso, S. Use and misuse of sorption kinetic data: A common mistake that should be avoided. *Adsorpt. Sci. Technol.* **2012**, *30*, 217–225. [CrossRef]
94. Weber, W. Kinetics of Adsorption on Carbon from Solution. *J. Sanit. Eng. Div.* **1963**, *89*, 31–60.
95. Low, M.J.D. Kinetics of chemisorption of gases on solids. *Chem. Rev.* **1960**, *60*, 267–312. [CrossRef]
96. Lente, G. *Deterministic Kinetics in Chemistry and Systems Biology: The Dynamics of Complex Reaction Networks*; Springer Briefs in Molecular Science; Springer International Publishing: Cham, Switzerland, 2015; ISBN 3319154826.
97. Chien, S.H.; Clayton, W.R. Application of Elovich Equation to the Kinetics of Phosphate Release and Sorption in Soils. *Soil Sci. Soc. Am. J.* **1980**, *44*, 265–268. [CrossRef]